

The effect of transformation twins on the seismic-frequency mechanical properties of polycrystalline $\text{Ca}_{1-x}\text{Sr}_x\text{TiO}_3$ perovskite

RICHARD J. HARRISON,* SIMON A.T. REDFERN, AND JOHN STREET

Department of Earth Sciences, University of Cambridge, Downing Street, Cambridge CB2 3EQ, U.K.

ABSTRACT

The low-frequency mechanical properties of polycrystalline $\text{Ca}_{1-x}\text{Sr}_x\text{TiO}_3$ ($0.5 \leq x \leq 0.9$) have been investigated as a function of temperature and bulk composition using the technique of dynamical mechanical analysis in three-point bend geometry. $\text{Ca}_{1-x}\text{Sr}_x\text{TiO}_3$ forms a cubic solid solution at high temperatures. At lower temperatures it undergoes successive displacive transitions to tetragonal and orthorhombic phases on cooling and increasing CaTiO_3 content. The low-frequency mechanical response of the tetragonal phase is dominated by thermally activated displacements of transformation twin domain walls, causing almost a twofold decrease in storage modulus relative to the twin-free cubic phase on cooling through the phase transition (superelastic softening). Below 140 °C the mobility of domain walls decreases and the storage modulus returns to a value close to that of the cubic phase. For $x > 0.85$, the cubic to tetragonal transition temperature is below 140 °C and domain walls are immobile immediately on formation, greatly reducing the magnitude of mechanical softening. The frequency dependence of the storage modulus is accurately described by a modified Burgers model of anelastic relaxation. Activation energies of 103 and 96 kJ/mol were obtained for samples with $x = 0.7$ and 0.74, respectively, suggesting that domain walls are strongly pinned by vacancies at the O positions. Superelastic softening is not observed below T_c for the tetragonal to orthorhombic phase transition in samples with $x = 0.5, 0.55,$ and 0.6. This is explained by the small value of the spontaneous strain in orthorhombic samples with intermediate compositions, which are distorted from cubic symmetry by less than 1%. With such small strain contrast between differently oriented twin domains, the effective force on the domain walls due to the external stress is less than the critical unpinning force, preventing displacement of the walls and suppressing superelastic softening.

INTRODUCTION

The attenuation of seismic waves is caused by the dissipation of strain energy as they propagate through an anelastic medium (anelasticity refers to a time-dependent but recoverable strain in response to an applied stress; Nowick and Berry 1972). By combining observations of seismic attenuation with a knowledge of the anelastic properties of minerals, the rheology of the inner Earth may be ascertained. However, the microscopic mechanisms responsible for anelasticity in the Earth's mantle remain controversial. The two currently favored theories attribute anelasticity in the upper mantle to either the movement of dislocations (e.g., anelastic unpinning) or grain-boundary processes (e.g., grain-boundary sliding) (Karato and Spetzler 1990; Jackson et al. 2003). Recently, however, an alternative mechanism has been proposed as a possible cause of seismic attenuation in the lower mantle from perovskite (Harrison and Redfern 2002). Measurements of the low-frequency mechanical properties of single-crystal LaAlO_3 revealed a tenfold decrease in modulus and a large increase in attenuation on cooling through the cubic to rhombohedral phase transition. This was explained by presence of transformation twins

in the rhombohedral phase, and their dynamical response to applied force.

Thermally activated displacement of domain walls provides a low-energy mechanism for developing macroscopic strain in response to an applied stress (Fig. 1). In the case of $\text{Ca}_{1-x}\text{Sr}_x\text{TiO}_3$, the cubic to tetragonal phase transition is accompanied by expansion of the structure along the crystallographic **c** axis and contraction along the **a** and **b** axes. The spontaneous strain is oriented differently in each twin domain. Those domains that are oriented favorably with respect to an applied stress have a lower free energy than those that are oriented unfavorably (e.g., a compressive stress applied along the length of the crystal in Figure 1 would lower the free energy of domain 2 with respect to domain 1, since the axis of contraction in domain 2 is parallel to the axis of compression). This produces an effective force on the domain wall, causing the favorably oriented domains to expand and the material as a whole to change length. The resulting macroscopic strain is determined by the spontaneous strain in each domain, the number of domain walls per unit length, and the distance moved by each wall (Harrison and Redfern 2002). The result is a dramatic reduction in modulus relative to that of the twin-free paraelastic phase, and an increase in energy dissipated due to the interaction between domain walls and lattice defects. This phenomenon, whereby

* E-mail: rjh40@esc.cam.ac.uk

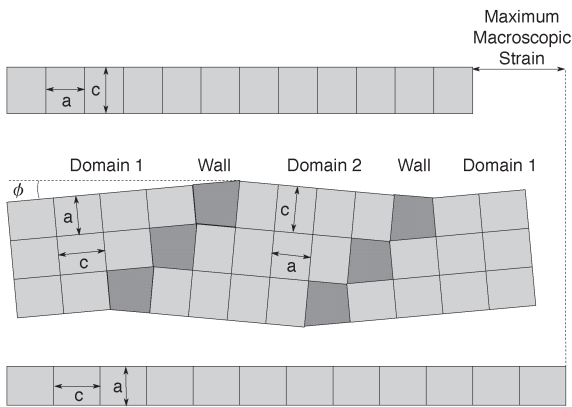


FIGURE 1. Schematic representation of differently oriented twin domains resulting from a cubic-tetragonal phase transition in perovskite. Unit cells in domain 1 have their long (c) axes aligned subparallel to the length of the sample, whereas those in domain 2 have their short (a) axes subparallel to the length. A compressive stress parallel to the length of the crystal would cause domain 2 to expand at the expense of domain 1, leading to a macroscopic decrease in length of the sample (top row of unit cells). A tensile stress parallel to the length of the crystal would cause domain 1 to expand at the expense of domain 2, leading to a macroscopic increase in length of the sample (bottom row of unit cells).

elastic deformations are mediated by changes in microstructure rather than the stretching of bonds, is termed “superelasticity” (Kityk et al. 2000).

Low-frequency mechanical properties are typically measured using the technique of dynamical mechanical analysis (DMA). Here we employ DMA in three-point bend geometry,

whereby the deflection of a thin strip of material in response to an alternating applied force is used to calculate the dynamic Young’s modulus (Schrantz 1997). The technique is used to determine the force, frequency, and temperature dependence of the low-frequency mechanical properties of polycrystalline $\text{Ca}_{1-x}\text{Sr}_x\text{TiO}_3$ ($0.5 \leq x \leq 0.9$). This material is a much closer structural and microstructural analogue of lower-mantle $(\text{Mg,Fe})(\text{Si,Al})\text{O}_3$ perovskite than the oriented single crystal samples of LaAlO_3 studied by Harrison and Redfern (2002). The use of polycrystalline samples with a range of bulk compositions enables us to determine how superelasticity and domain-wall pinning are affected by the presence of grain boundaries and chemical substitutions. Samples with $x < 0.65$ are orthorhombic at room temperature and transform first to tetragonal and then to cubic symmetry on heating, allowing us to study for the first time the effect on superelasticity of heating and cooling through two successive displacive phase transitions.

PHASE TRANSITIONS IN $\text{Ca}_{1-x}\text{Sr}_x\text{TiO}_3$

Phase transitions in $\text{Ca}_{1-x}\text{Sr}_x\text{TiO}_3$ have been studied extensively (Fig. 2). The CaTiO_3 end-member is orthorhombic ($Pnma$) at room temperature and transforms to a tetragonal structure ($I4/mcm$) at 1227 °C and to the ideal cubic perovskite structure ($Pm\bar{3}m$) at 1310 °C (Redfern 1996; Kennedy et al. 1999). The orthorhombic and tetragonal structures are related to the cubic structure via tilting of the TiO_6 octahedra (corresponding to tilt systems $a^+b^-b^-$ and $a^0a^0c^-$, respectively, in the classification of Glazer 1972). The SrTiO_3 end-member is cubic ($Pm\bar{3}m$) at room temperature and transforms to the tetragonal ($I4/mcm$) structure below 106 K (Cowley 1996; Salje et al. 1998; Hayward and Salje 1999).

The sequence of phase transitions as a function of temperature and bulk composition in the solid solution has been stud-

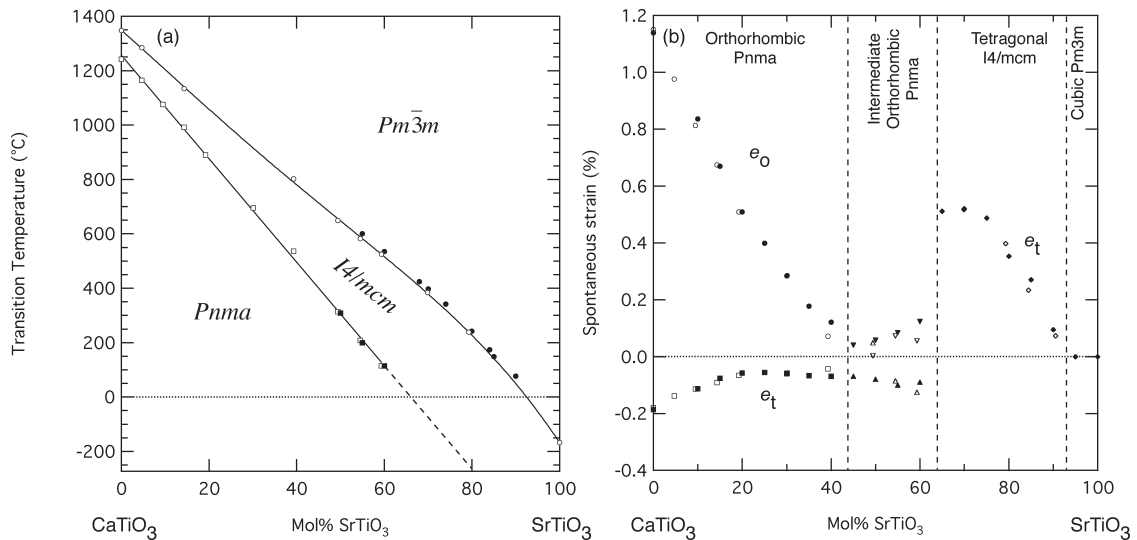


FIGURE 2. (a) Phase diagram for the $\text{Ca}_{1-x}\text{Sr}_x\text{TiO}_3$ solid solution. Open circles and open squares show $T_c^{c \rightarrow t}$ and $T_c^{t \rightarrow o}$, respectively (after Qin et al. 2000). Closed circles and squares show $T_c^{c \rightarrow t}$ and $T_c^{t \rightarrow o}$ derived from the DMA results of this study. Solid lines are guides to the eye. Dashed line is a linear extrapolation of the $T_c^{t \rightarrow o}$ data. (b) Spontaneous strain at room temperature as a function of bulk composition in the $\text{Ca}_{1-x}\text{Sr}_x\text{TiO}_3$ solid solution (after Carpenter et al. 2001). Note the steady decrease in orthorhombic distortion (e_o) with increasing x and the small value of the spontaneous strains in the intermediate orthorhombic phase from $0.45 < x < 0.65$.

ied by Ball et al. (1998), Qin et al. (2000), Ranjan et al. (1999), Ranjan and Pandey (1999, 2001a, 2001b), and Yamanaka et al. (2002). Figure 2a illustrates the results of Qin et al. (2000), which are in good agreement with those of Ball et al. (1998). The cubic to tetragonal transition temperature (T_c^{c-t}) decreases linearly with increasing x until around $x \sim 0.9$, whereafter it decreases more rapidly. Such behavior is interpreted as the influence of quantum fluctuations at low temperatures, which stabilize the high-temperature cubic phase and suppress the transition temperature (Hayward and Salje 1998). The tetragonal to orthorhombic transition temperature (T_c^{t-o}) similarly decreases linearly with increasing x . At room temperature, samples with $x < 0.65$ are predicted to be orthorhombic, those with $0.65 < x < 0.92$ are predicted to be tetragonal, and those with $x > 0.92$ are predicted to be cubic.

An unusual variation in the room-temperature lattice parameters as a function of composition was identified by Ball et al. (1998) and Qin et al. (2000). The results of Qin et al. (2000) are shown in Figure 2b in the form of symmetry-adapted components of spontaneous strain relative to a hypothetical room-temperature cubic phase (Carpenter et al. 2001). The orthorhombic distortion observed in CaTiO_3 (dominated by the spontaneous strain component e_o) decreases smoothly with increasing x , until the lattice parameters converge at about $x = 0.45$ to give a pseudo-tetragonal metric with very small spontaneous strain. This convergence was initially taken as evidence of a phase transition from $Pnma$ to an intermediate orthorhombic phase with space group $Cmcm$. Electron diffraction measurements later showed this space group assignment to be incorrect (Howard et al. 2001), and although the intermediate phase does appear to be structurally distinct from CaTiO_3 , it has the same $Pnma$ space group. The intermediate phase extends from $0.45 < x < 0.65$, whereafter the tetragonal ($I4/mcm$) phase is stable and the spontaneous strain (dominated by the component e_t) increases suddenly. The structural nature of the intermediate phase remains unknown.

EXPERIMENTAL PROCEDURES

Sample preparation

Samples with bulk compositions $0.68 < x < 0.9$ were taken from the combined XRD and DSC study of Qin et al. (2000), and a detailed description of the sample preparation and characterization can be found therein. Starting materials were synthesized by drying CaCO_3 and SrCO_3 at 500°C and TiO_2 at 1000°C for 3 hours. Stoichiometric mixtures were then heated at 1300°C for four hours, ground in an agate mortar, pressed into pellets, and fired in air at 1600°C for 48 hours with periodic regrinding and repressing. The resulting samples were sintered polycrystalline pellets, homogeneous at the 1% level. Samples with $0.5 < x < 0.6$ were synthesized using the same method at the Research School of Earth Sciences, Australia National University.

Dynamical mechanical analysis

Mechanical properties have been measured using a Perkin-Elmer dynamical mechanical analyser (DMA-7) operating in three-point bend geometry (Menard 1999). The principle of

DMA is illustrated in Figure 3. The sample is a polycrystalline beam with length l , width w , and thickness t , suspended on two knife-edges (Fig. 3a). A force is applied to the sample from above via a third knife-edge located halfway along its length. The applied force has a static component (F_s), which ensures that the sample remains in contact with the knife edges at all times, and a dynamic component (F_D) with frequency (f) in the range 0.01–50 Hz. The amplitude (u) and phase lag (δ) of the mechanical response are measured via inductive coupling with a resolution of $\Delta u \sim 10$ nm and $\Delta\delta \sim 0.1^\circ$, respectively (Fig. 3b). The amplitude of displacement is a function of both the Young's (Y) and shear (G) moduli, but in three-point bend geometry the contribution from the shear modulus vanishes for $l \gg t$ (Kityk et al. 2000). Under these conditions, the dynamic Young's modulus parallel to the sample length is simply related to the dynamic force and the amplitude of deflection (u_D) via:

$$Y = \frac{l^3}{4t^3w} \frac{F_D}{u_D} \exp(i\delta) \quad (1)$$

The real ($Y' = |Y| \cos\delta$) and imaginary ($Y'' = |Y| \sin\delta$) components of the dynamic modulus are referred to as the storage and loss moduli, respectively. The ratio $Y''/Y' = \tan\delta$ is the attenuation (energy dissipated per cycle). This quantity is often referred to as Q^{-1} (inverse quality factor) in the geophysics literature. A perfectly elastic material has $\tan\delta = 0$, whereas an anelastic material has $\tan\delta > 0$. The sample assembly is encased in a resistance furnace, permitting measurement up to a temperature of $\sim 650^\circ\text{C}$. The absolute accuracy of the values of moduli obtained is affected by measurement errors, zero errors, and systematic offsets within the apparatus, and is therefore relatively low (10–20%). This means that the technique is not suitable for determining absolute values of the elastic constants. However, the relative precision is better than 1%, allowing changes in mechanical properties as a function of force, frequency, and temperature to be determined with a high degree of sensitivity. For this reason, comparisons between different DMA experiments are usually made in terms of the relative modulus.

Three different types of experiment can be performed; temperature scans, frequency scans, and dynamic force scans. In a temperature scan, F_s , F_D , and f are held constant, while the temperature (T) is moved up or down at a rate of $5^\circ\text{C}/\text{min}$. The furnace operates with a continuous purge of dry N_2 gas, and temperatures are calibrated against the melting points of high-purity metal standards. Values of the storage modulus and $\tan\delta$

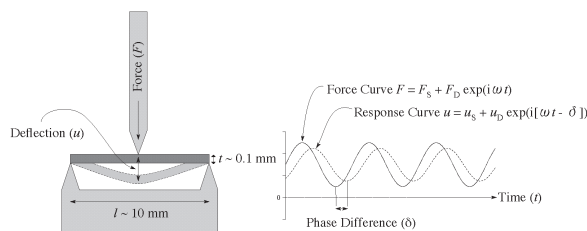


FIGURE 3. (a) Three-point bend geometry of the DMA-7. (b) Dynamic force and response signals during dynamical mechanical analysis.

are recorded continuously and then averaged into temperature bins of chosen width (typically 1–5 °C). F_D is set to a value of approximately $0.9 F_S$, so that the minimum and maximum forces on the sample are $0.1 F_S$ and $1.9 F_S$, respectively. Values for F_S are typically in the range 100–500 mN. All temperature scans were performed at a frequency of 1 Hz. In a frequency scan, F_S , F_D , and T are held constant while f is swept between 0.1 and 50 Hz. The rate of the frequency sweep is automatically controlled by the data collection software and varies between 0.04 Hz/min at low frequencies and 4 Hz/min at high frequencies. In a dynamic force scan, T and f are held constant while F_D is swept between 50 and 500 mN at a rate of 10 mN/min. In these experiments, F_S was programmed to maintain a value of $1.2 F_D$ at all times.

RESULTS

Mechanical properties as a function of temperature

Figure 4 shows the storage modulus (closed circles) and $\tan\delta$ (open circles) as a function of temperature for sample CST70 (bulk composition $\text{Ca}_{0.3}\text{Sr}_{0.7}\text{TiO}_3$) on cooling from 500 °C to room temperature. The large decrease in storage modulus below 400 °C and the corresponding increase below 140 °C occur at the boundaries between different regimes of mechanical behavior (Harrison and Redfern 2002). The paraelastic regime ($T > T_c^{c-1}$) corresponds to the stability field of the high-symmetry paraelastic phase. In this regime the material is untwinned, $\tan\delta$ is essentially zero (indicating ideal elastic be-

havior), and the storage modulus corresponds to the intrinsic Young's modulus of the cubic phase. In the ideal case, the storage modulus is either constant or decreases slightly with increasing temperature in the paraelastic regime due to the weakening effect of thermal expansion. In some cases, however, a small degree of elastic softening occurs as T_c^{c-1} is approached from above due to coupling between the spontaneous strain and order-parameter fluctuations (Carpenter and Salje 1998). This may be the cause of the positive slope of the modulus vs. temperature curve in the paraelastic regime observed in Figure 4.

The start of the superelastic regime ($T < T_c^{c-1}$) coincides with the cubic to tetragonal phase transition and the formation of transformation twins. If the temperature is high enough, thermal energy is sufficient to allow domain walls to move in response to an applied stress and the modulus rapidly decreases to a value almost half that of the cubic phase. The modulus remains constant throughout the majority of the superelastic regime, in agreement with the model of superelasticity derived by Harrison and Redfern (2002) to explain similar behavior in single-crystal LaAlO_3 . The formation of mobile domain walls is accompanied by an abrupt increase in $\tan\delta$, as energy is dissipated by moving domain walls against the frictional force exerted by lattice defects (there may also be a small contribution due to the Peierls force associated with moving a wall of finite thickness through a discrete lattice; Wang et al. 1996; Meyer and Vanderbilt 2002). The linearity of the force-deflection curves in the superelastic regime was investigated by performing dynamic force scans at a range of temperatures. In stark contrast to the highly non-linear behavior observed in single-crystal LaAlO_3 , the mechanical response of the polycrystalline samples was found to be linear over the dynamic force range $50 \text{ mN} < F_D < 500 \text{ mN}$.

The domain-freezing regime sets in at some temperature below T_c^{c-1} (around 140 °C in this case; Fig. 4). Domain wall motion is anelastic, with a time-dependence that results from wall-wall, wall-surface, and wall-defect interactions. In the domain-freezing regime, the relaxation time for domain wall motion (a measure of the time required for walls to move to their equilibrium positions on application of a constant stress) increases according to the Arrhenius relationship:

$$\tau = \tau_0 \exp[E/RT] \quad (2)$$

where E is an activation energy. This leads to an anelastic relaxation phenomenon (Nowick and Berry 1972), manifested by a pronounced resonance peak in $\tan\delta$ and a rise in modulus from the relaxed value observed in the superelastic regime (i.e., when $\omega\tau \ll 1$, where $\omega = 2\pi f$ is the angular frequency of the DMA experiment) to the unrelaxed value observed at low temperatures (i.e., when $\omega\tau \gg 1$). For $\omega\tau \gg 1$, walls are unable to unpin themselves on the timescale of the dynamic force, and so are effectively frozen. The unrelaxed modulus may be significantly lower than the intrinsic modulus of the cubic phase due to the combined effects of order parameter-strain coupling and the ability of domain walls to bend between pinning sites. The maximum in $\tan\delta$ occurs at the resonance frequency (i.e., when $\omega\tau = 1$). This point is used as an arbitrary definition of the freezing temperature T_f .

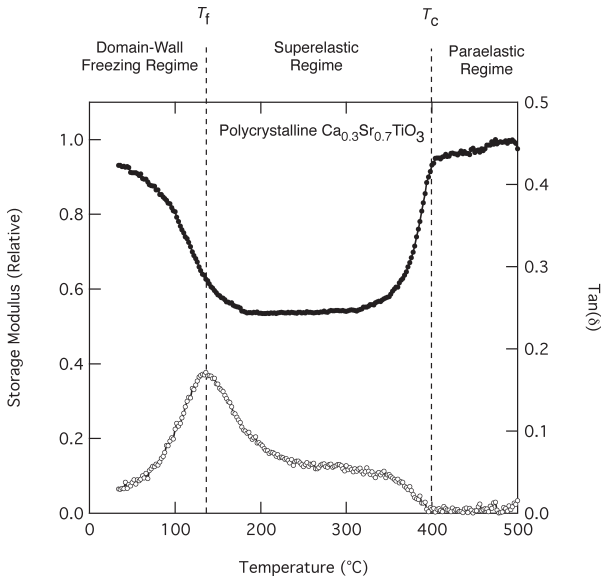


FIGURE 4. Relative storage modulus, Y' (closed symbols), and attenuation, $\tan\delta$ (open symbols), as a function of temperature for polycrystalline $\text{Ca}_{0.3}\text{Sr}_{0.7}\text{TiO}_3$. Operating conditions $F_S = 120 \text{ mN}$, $F_D = 108 \text{ mN}$, $f = 1 \text{ Hz}$. Dashed lines show the boundaries between the paraelastic regime (cubic symmetry, no twins), the superelastic regime (tetragonal symmetry, mobile domain walls), and the domain-freezing regime (tetragonal symmetry, twins immobile on the time scale of the dynamic force).

Mechanical properties as a function of composition ($0.68 \leq x \leq 0.9$)

Mechanical properties as a function of temperature for several samples in the range $0.68 < x < 0.9$ (for which the tetragonal structure is the stable phase at room temperature) are summarized in Figure 5. For compositions in the range $0.68 < x < 0.8$, the mechanical behavior in the three regimes is similar to that described in Figure 4. The drop in modulus at the boundary between the paraelastic and superelastic regimes occurs at progressively lower temperatures with increasing x , following the trend of T_c^{c-t} vs. x determined independently from XRD and DSC measurements (Qin et al. 2000; Ball et al. 1998). The sudden increase in $\tan\delta$ on entering the superelastic regime provides a sensitive method of determining T_c^{c-t} , as shown by the excellent agreement between DMA-derived (closed circles) and the DSC-derived (open circles) values in Figure 2a.

In contrast to the steadily decreasing value of T_c^{c-t} with increasing x , T_f is essentially independent of composition, with values typically in the range 130–140 °C. The maximum value of $\tan\delta$ decreases with increasing Sr content, and there is a commensurate decrease in the magnitude of superelastic softening as the composition approaches $x = 0.85$ (the point at which $T_c^{c-t} \sim T_f$). For $x > 0.85$, $T_c^{c-t} < T_f$ and domain walls are effectively frozen immediately on formation, eliminating the superelastic regime. The softening measured in these samples is related mainly to the “intrinsic” elastic softening due to order parameter-strain coupling (Carpenter and Salje 1998). A drop in modulus of $\sim 10\%$ is observed in sample CST90, which gives some indication of the relative magnitudes of the intrinsic and superelastic softening effects in these materials.

The mechanical behavior of sample CST85 is shown in more detail in Figure 6. This sample shows evidence for a second anelastic relaxation process at temperatures below T_f , which leads to an increase in modulus and a second peak in $\tan\delta$ at 60 °C. This behavior was reproducible during repeated heating and cooling cycles, but was not seen in other samples of simi-

lar composition (e.g., sample CST84 in Fig. 5). The origin of this anomalous behavior is unknown.

Mechanical properties as a function of composition ($0.5 \leq x \leq 0.6$)

Mechanical properties as a function of temperature for samples in the range $0.5 \leq x \leq 0.6$ (for which the orthorhombic structure is the stable phase at room temperature) are summarized in Figure 7. The behavior on cooling through the high-temperature cubic to tetragonal phase transition is equivalent to that observed in Figure 5 for samples with $x < 0.85$. The paraelastic regime was not observed in CST50 (Fig. 7c), since T_c^{c-t} for this bulk composition is slightly higher than the maximum temperature achievable in the DMA apparatus.

Mechanical behavior at lower temperatures differs significantly from that observed in more Sr-rich compositions due to the influence of the tetragonal to orthorhombic phase transition. The effect is most pronounced in CST50, where the phase transition occurs at a temperature much higher than T_f (Fig. 7c). The modulus jumps from its relaxed to its unrelaxed value and $\tan\delta$ is reduced to zero immediately on cooling through T_c^{t-o} (314 °C). This sudden change in mechanical properties is consistent with the first-order nature of the tetragonal to orthorhombic phase transition. Similar behavior, although less sharp, is observed in CST60 and CST55 (Figs. 7a and b). In each case, the increase in modulus and decrease in $\tan\delta$ correlate with the tetragonal to orthorhombic phase transition (closed squares in Fig. 2a), and shouldn't be confused with the effects of anelastic relaxation observed in more Sr-rich samples at similar temperatures. These measurements suggest that superelasticity is strongly suppressed in the intermediate orthorhombic phase.

Frequency dependence of mechanical properties

To determine a value for the activation energy for domain wall motion, the frequency-dependence of the storage modu-

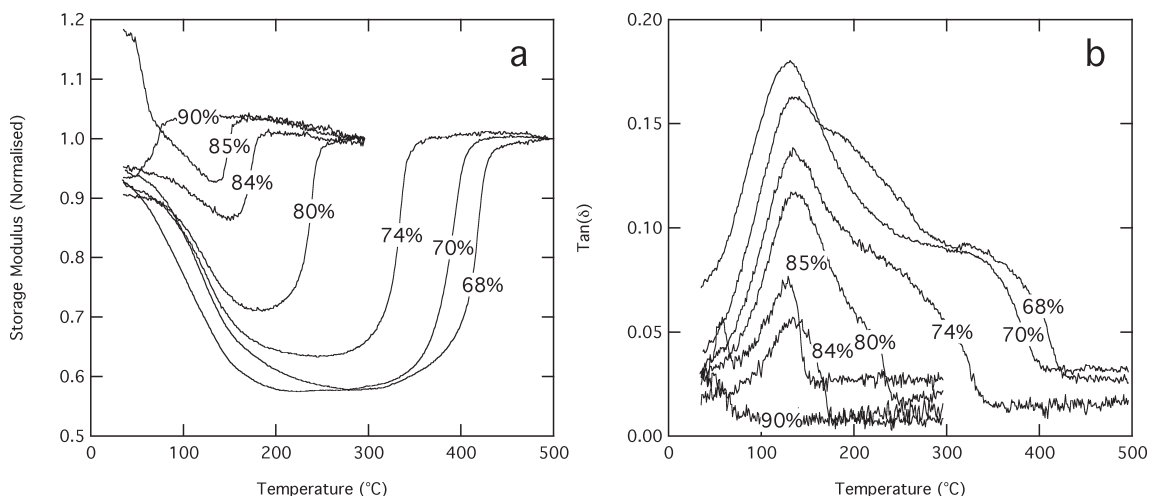


FIGURE 5. (a) Relative storage modulus and (b) $\tan\delta$ as a function of temperature for several samples of the $\text{Ca}_{1-x}\text{Sr}_x\text{TiO}_3$ solid solution. Percentages refer to the proportion of SrTiO_3 in the solid solution. Operating conditions $F_s = 500$ mN, $F_D = 450$ mN, $\omega = 1$ Hz.

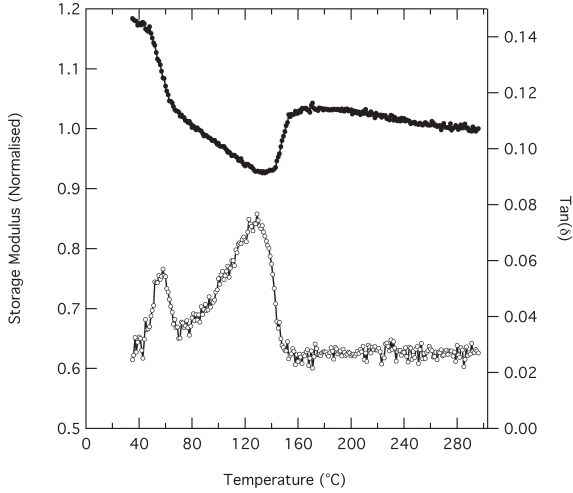


FIGURE 6. Relative storage modulus (closed symbols), and $\tan\delta$ (open symbols) as a function of temperature for polycrystalline $\text{Ca}_{0.15}\text{Sr}_{0.85}\text{TiO}_3$. Operating conditions $F_S = 500$ mN, $F_D = 450$ mN, $\omega = 1$ Hz.

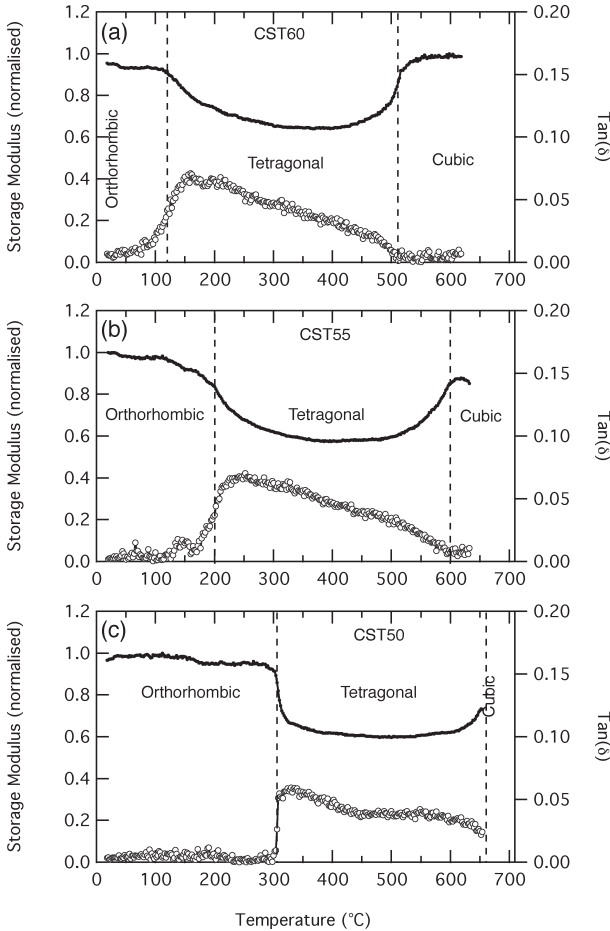


FIGURE 7. Relative storage modulus (closed symbols), and $\tan\delta$ (open symbols) as a function of temperature for polycrystalline (a) $\text{Ca}_{0.4}\text{Sr}_{0.6}\text{TiO}_3$, (b) $\text{Ca}_{0.45}\text{Sr}_{0.55}\text{TiO}_3$, and (c) $\text{Ca}_{0.5}\text{Sr}_{0.5}\text{TiO}_3$. Dashed lines mark the approximate positions of the cubic-tetragonal and tetragonal-orthorhombic phase transitions.

lus was measured at a range of temperatures spanning the boundary between the domain-freezing and superelastic regimes (100 to 300 °C) in samples CST74 and CST70. Instrumental contributions to the frequency-dependent signal were determined by averaging data collected at temperatures in the centre of the superelastic regime (where the modulus is observed to be independent of temperature). This instrumental baseline was then subtracted from all measurements, isolating the anelastic contribution to the frequency-dependent signal caused by domain-wall motion. The results for sample CST74 are shown in Figure 8.

The frequency dependence of the modulus is very similar to that observed in single-crystal LaAlO_3 (Harrison and Redfern 2002) and can be modeled quantitatively using a modified Burgers model of a linear viscoelastic solid (Jackson 2000; Karato and Spetzler 1990). The Burgers model describes the measured system in terms of an analogue of elastic springs and viscous dashpots in series and parallel combinations. The response function under constant stress, σ , is given by:

$$J(t) = \frac{e(t)}{\sigma} = J_U + \delta J [1 - \exp(-t/\tau)] + \frac{t}{\eta} \quad (3)$$

where $J(t)$ is the compliance, $e(t)$ is the strain, J_U and δJ are the instantaneous (elastic) and the time-dependent (anelastic) contributions to the compliance, τ is the anelastic relaxation time

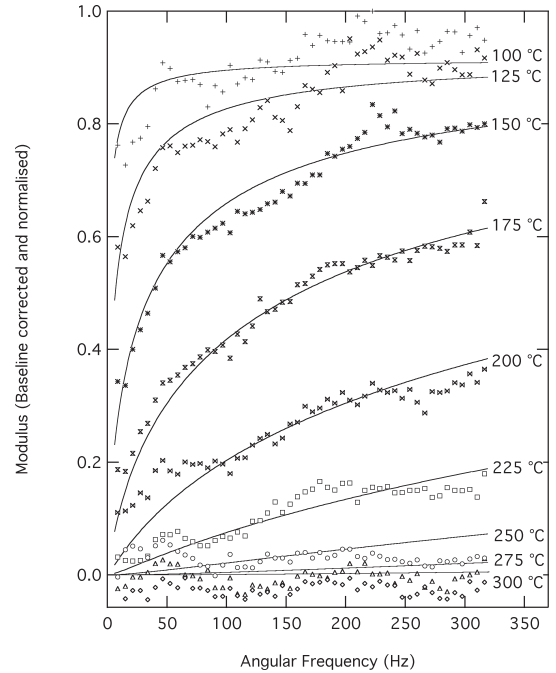


FIGURE 8. Frequency-dependence of the storage modulus (symbols) at various temperatures spanning the domain-freezing and superelastic regimes for a sample of bulk composition $\text{Ca}_{0.26}\text{Sr}_{0.74}\text{TiO}_3$. A non-linear instrumental baseline has been subtracted from all data before normalization. Solid lines represent the results of a fit of the data at all temperatures simultaneously, using the modified Burgers model (Eq. 9). Fit parameters are $E_{av} = 96(1)$ kJ/mol, $\delta E = 7(2)$ kJ/mol, and $\tau_0 = 8(2) \times 10^{-14}$ s.

(Eq. 2), and η is the steady-state Newtonian viscosity (not required for a purely anelastic relaxation). For an alternating stress with angular frequency ω , the corresponding dynamic compliance, $J(\omega)$ is given by (Jackson 2000):

$$J(\omega) = J_U + \frac{\delta J}{(1 + i\omega\tau)} - \frac{i}{\eta\omega} \quad (4)$$

with real and imaginary components $J_1(\omega)$ and $J_2(\omega)$, respectively:

$$J_1(\omega) = J_U + \frac{\delta J}{(1 + \omega^2\tau^2)} \quad (5)$$

$$J_2(\omega) = \frac{\omega\tau\delta J}{(1 + \omega^2\tau^2)} + \frac{1}{\eta\omega} \quad (6)$$

Equations 5 and 6 describe the relationships between relaxed modulus, unrelaxed modulus, and mechanical loss in an anelastic solid. They explain the observation that the maximum in $\tan\delta$ and δJ are proportional, as seen in Figure 5. In a real material it is usually found that a distribution of characteristic relaxation times is required to fit the experimental data, implying a range in activation energies for the viscous components of the model. Attempts to model our frequency- and temperature-dependent data using a single activation energy implied domain wall freezing over much too narrow a temperature range. We have therefore modified the Burgers model to account for a Gaussian distribution of activation energies, $D(E)$:

$$D(E) = \frac{1}{\delta E\sqrt{2\pi}} \exp\left(-\frac{(E - E_{av})^2}{2\delta E^2}\right) \quad (7)$$

where E_{av} is the average activation energy and δE is the standard deviation from the mean. The response function then becomes (Jackson 2000):

$$J(t) = \frac{e(t)}{\sigma} = J_U \left\{ 1 + \Delta \int_0^\infty D(E) \left[1 - \exp\left(-\frac{t}{\tau_0 \exp(E/RT)}\right) \right] dE \right\} + t/\eta \quad (8)$$

where Δ is the relaxation strength (ratio of anelastic to elastic strain). The real and imaginary components are:

$$J_1(\omega) = J_U \left\{ 1 + \Delta \int_0^\infty \frac{D(E)dE}{1 + \omega^2[\tau_0 \exp(E/RT)]^2} \right\} \quad (9)$$

$$J_2(\omega) = \omega J_U \Delta \left\{ \int_0^\infty \frac{\tau_0 \exp(E/RT) D(E)dE}{1 + \omega^2[\tau_0 \exp(E/RT)]^2} \right\} + \frac{1}{\eta\omega} \quad (10)$$

Equation 9 has been used to fit the frequency-dependent measurements at all temperatures simultaneously, yielding values of $E_{av} = 96(1)$ kJ/mol, $\delta E = 7(2)$ kJ/mol, and $\tau_0 = 8(2) \times 10^{-14}$ s for CST74. The results of the fit are shown as the solid lines in Figure 8. Values of $E_{av} = 103(1)$ kJ/mol, $\delta E = 9(2)$ kJ/mol, and $\tau_0 = 5(2) \times 10^{-15}$ s were obtained from similar measurements of sample CST70.

DISCUSSION

The results presented here provide a useful comparison with those reported previously for single-crystal LaAlO₃ (Harrison

and Redfern 2002). The important similarities and differences between these two studies provide new insight into the phenomenon of microstructure-related anelasticity in perovskite, and are discussed in turn below.

Magnitude of superelastic softening

Although the magnitude of superelastic softening observed in the present study is large (at least a factor of four larger than the elastic softening associated with order parameter-strain coupling), the effect is greater still in single-crystal LaAlO₃, where the effective storage modulus decreases by a factor of ten below the cubic to rhombohedral phase transition. This difference is simply explained by the variation of the force on a domain wall with the orientation of the applied stress. Consider the spontaneous strain e^A_{ij} and e^B_{ij} associated with two domains A and B in a tetragonally distorted structure:

$$e^A_{ij} = \begin{pmatrix} 2e & 0 & 0 \\ 0 & -e & 0 \\ 0 & 0 & -e \end{pmatrix} \quad e^B_{ij} = \begin{pmatrix} -e & 0 & 0 \\ 0 & 2e & 0 \\ 0 & 0 & -e \end{pmatrix} \quad (11)$$

Domains A and B are elongated parallel to [100] and [010] of the high-temperature cubic phase, respectively, and the domain wall separating them is parallel to either (110) or ($\bar{1}$ 10). For a uniaxial stress, σ , applied in a general direction, the stress tensor in a particular grain is given by:

$$\sigma_{ij} = \sigma a_i a_j \quad (12)$$

where a_i are direction cosines defining the orientation of σ relative to the crystallographic axes of the high-temperature cubic phase. Ignoring the ferrobielastic contribution, the force per unit area on the domain wall is equal to the free energy difference per unit volume between the two domains:

$$\Delta G = e^A_{ij} \sigma_{ij} - e^B_{ij} \sigma_{ij} = 3e\sigma(a_1^2 - a_2^2) \quad (13)$$

This equation is plotted in Figure 9a as a function of orientation for uniaxial stresses applied within the (001) plane. The force is zero when the stress is applied parallel or perpendicular to the domain wall and the force is maximum when the stress is applied at 45° to the domain wall. The superelastic contribution to the elastic compliance (δJ , see Eq. 3) was derived for the two-domain case of a cubic to rhombohedral transition by Harrison and Redfern (2002). The equivalent expression for a cubic to tetragonal transition is:

$$\delta J = \frac{t^2(a_1^2 - a_2^2)^2}{8l^2 C} \quad (14)$$

where C is a constant describing the strength of the restoring force acting on the domain walls (the restoring force can be due to wall-defect, wall-wall, or wall-surface interactions, or alternatively due to the compatibility strain associated with rotating the wall away from its preferred orientation). The storage modulus is given by:

$$Y^{-1} = J_U + \frac{t^2(a_1^2 - a_2^2)^2}{8l^2 C} \quad (15)$$

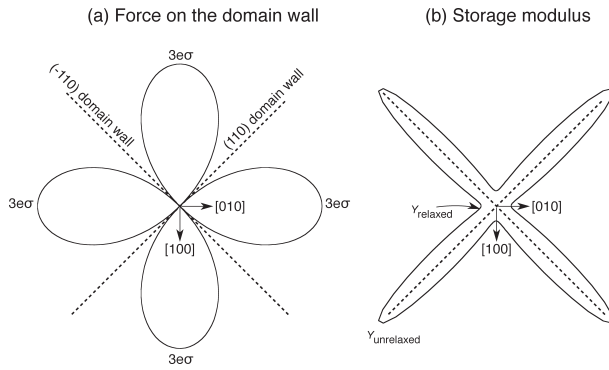


FIGURE 9. (a) Polar plot of the effective force per unit area on a (110) or (−110) domain wall as a function of the orientation of uniaxial stress, σ , applied within the (001) plane. The maximum force of $3\epsilon\sigma$ (where ϵ is the spontaneous strain) occurs for stresses applied at 45° to the domain wall. Force is zero for stresses applied parallel or perpendicular to the wall. (b) Corresponding polar plot of storage modulus as a function of orientation, assuming a factor-of-ten difference between the relaxed and unrelaxed moduli (as observed in single crystals of LaAlO_3 ; Harrison and Redfern 2002). The average value of the modulus in a polycrystal of twinned grains will be intermediate between the relaxed and unrelaxed values. The massive anisotropy of twinned grains provides a potential source of seismic anisotropy in rocks with small degrees of preferred orientation.

This equation is plotted in Figure 9b with values $J_U = 0.1$ and $t^2/8PC = 1$, giving a factor of ten difference between the maximum and minimum moduli. This factor of ten corresponds to the difference between the maximum (unrelaxed) and minimum (relaxed) moduli observed by Harrison and Redfern (2002), where the domain walls were in the optimum orientation relative to the applied stress. In a polycrystalline aggregate, the storage moduli of individual grains will be evenly distributed between the unrelaxed and relaxed values. The average modulus (whose upper and lower bounds are determined by the Voigt and Reuss averages) will have some intermediate value. Figure 9b gives an indication of the massive mechanical anisotropy observable in a grain containing domain walls in a single orientation. If the grains are evenly distributed over all orientations, then the mechanical properties as a whole will be isotropic. However, given the large intrinsic anisotropy of twinned grains, even a small degree of preferred orientation will be sufficient to impart significant seismic anisotropy to the material as a whole.

Domain-freezing temperature

Comparing the domain-freezing temperature observed in a single crystal with that observed in polycrystalline samples of varying bulk composition provides some insight into the mechanism of domain wall pinning. Possible pinning mechanisms include the interaction between domain walls and defects such as grain boundaries, dislocations, surfaces, and cation and anion vacancies. Alternatively, domain walls may be pinned by the inhomogeneous strain fields associated with the substitution of differently sized Ca and Sr cations in the solid solution.

As shown in Figure 5, T_i is independent of bulk composition, with typical values in the range $130\text{--}140^\circ\text{C}$. The strain fields associated with chemical substitution in solid solutions vary strongly with bulk composition (Carpenter and Boffa Ballaran 2001). It is unlikely, therefore, that these strain fields play a dominant role in the pinning of domain walls. The fact that very similar values of T_i ($150\text{--}170^\circ\text{C}$) are observed in single-crystal LaAlO_3 implies that the effect of grain boundaries and the sample surface is also negligible. The most likely source of pinning is, therefore, intrinsic defects common to both types of sample, such as cation and anion vacancies. The activation energies of 96, 103, and 84 kJ/mol observed in CST74, CST70, and LaAlO_3 , respectively, all correspond closely to the activation energy for diffusion of vacancies at O sites (Warren et al. 1996). This strongly suggests that domain walls are pinned by O atom vacancies and that the rate-determining step in the unpinning mechanism involves the short-range diffusion of O atom vacancies. This conclusion is in agreement with several mechanical and dielectric loss studies of perovskites and other oxide ceramics (Wang et al. 2001; Yan et al. 1999; Wang and Fang 2002). Wang et al. (2001) demonstrated a correlation between the height of the relaxational $\tan\delta$ peak and the concentration of O atom vacancies in samples of $\text{Pb}(\text{Zr}_{0.52}\text{Ti}_{0.48})\text{O}_3$ perovskite annealed under different O atom fugacities.

Temperature-independence of the superelastic modulus

Another important similarity between the behavior of polycrystalline and single-crystal samples is the temperature-independence of the relaxed modulus in the superelastic regime (Fig. 4). Kityk et al. (2000) observed that the superelastic modulus in single-crystal SrTiO_3 scaled with the spontaneous strain, such that $Y \propto e^{-1} \propto Q^{-2} \propto (T_c - T)^{-1}$. This behavior was later shown to be the result of saturation, whereby adjacent domain walls come into contact with each other at high values of the applied force (Harrison and Redfern 2002). As long as the dynamic force is small enough to prevent saturation, the superelastic contribution to the elastic compliance is independent of the spontaneous strain (Eq. 14) and, therefore, independent of temperature. The strain independence arises because the restoring force on a displaced domain wall is proportional to the square of the spontaneous strain. This counteracts the fact that both the driving force for wall displacement (Eq. 13) and the macroscopic strain due to wall displacement (Fig. 1) are proportional to the spontaneous strain.

Temperature-independence of the superelastic modulus was observed in the polycrystalline samples up to dynamic forces of 500 mN, indicating that saturation does not occur up to this value of the force. A similar conclusion was drawn from dynamic force scans obtained in the superelastic regime, which showed linear (unsaturated) mechanical behavior up to 500 mN. In contrast, the single-crystal LaAlO_3 sample saturated readily at forces greater than 300 mN. This difference is most likely due to the smaller superelastic strain induced in the polycrystalline samples, where the response of individual grains depends upon their orientation with respect to the applied force. It may also be explained by a greater spacing between neighboring domain walls in the polycrystalline samples.

Loss of superelasticity in the intermediate orthorhombic phase

Given that the superelastic modulus is predicted to be independent of the spontaneous strain (Eq. 14; Harrison and Redfern 2002), the transition from the tetragonal phase to the intermediate orthorhombic phase (which is accompanied by a sudden decrease in spontaneous strain; Fig. 2b) should have little effect on the mechanical behavior. This is clearly not the case (Fig. 7). Since electron microscopy studies demonstrate that domain walls are still present in the intermediate orthorhombic phase (Howard et al. 2001), we conclude that these walls are immobile. Equation 14 is only valid when twins are free to move under the application of *any* force (i.e., pinning is neglected). However, Harrison and Redfern (2002) identified a critical force, F_{crit} , below which domain walls were unable to escape their pinning sites. As long as the force on the domain walls exceeds F_{crit} then Equation 14 holds, and the superelastic modulus is independent of the spontaneous strain. If the spontaneous strain becomes too small, however, the net force on the domain walls (Eq. 13) is less than F_{crit} and the superelastic softening is lost. The origin of the small spontaneous strain in the intermediate orthorhombic phase remains to be explained.

We have shown that superelasticity and domain wall freezing are important aspects of the low-frequency mechanical response of polycrystalline perovskite, associated with the transformations from cubic to lower-symmetry structures. $Ca_{1-x}Sr_xTiO_3$ perovskites have received much attention in the past due to their transition behavior, which is assumed to be a good analogue of the behavior of isostructural $(Mg,Fe)SiO_3$ perovskite in the lower mantle. Our results show that low-symmetry polycrystalline perovskite is anelastic, and the frequency and temperature dependence of anelasticity can be understood within the framework of the Burgers model. The role of O atom vacancies in pinning wall motion in perovskite is intriguing, and we are now undertaking further experimental and computational studies of defect-bearing perovskites to further elucidate the mechanisms of wall pinning in the perovskite structure.

ACKNOWLEDGMENTS

This study was funded by the EPSRC under grant GR/M49816. The authors are grateful to J. Scott and K.H. Salje for useful discussions.

REFERENCES CITED

- Ball, C.J., Begg, B.D., Cookson, D.J., Thorogood, G.J., and Vance, E.R. (1998) Structures in the system $CaTiO_3/SrTiO_3$. *Journal of Solid State Chemistry*, 139, 238–247.
- Carpenter, M.A. and Boffa Ballaran, T. (2001) The influence of elastic strain heterogeneities in silicate solid solutions. In C. Geiger, Ed., *European Mineralogical Union Notes in Mineralogy*, Vol. 3., Eötvös University Press, Budapest.
- Carpenter, M.A. and Salje, E.K.H. (1998) Elastic anomalies in minerals due to structural phase transitions. *European Journal of Mineralogy*, 10, 693–812.
- Carpenter, M.A., Becerro, A.I., and Seifert, F. (2001) Strain analysis of phase transitions in $(Ca,Sr)TiO_3$ perovskites. *American Mineralogist*, 86, 348–363.
- Cowley, R.A. (1996) The phase transition in strontium titanate. *Philosophical transactions of the Royal Society of London A*, 354, 2799–2814.
- Glazer, A.M. (1972) The classification of tilted octahedra in perovskites. *Acta Crystallographica*, B28, 3384–3392.
- Harrison, R.J. and Redfern, S.A.T. (2002) The influence of transformation twins on the seismic-frequency elastic and anelastic properties of perovskite: Dynamical mechanical analysis of single-crystal $LaAlO_3$. *Physics of the Earth and Planetary Interiors*, 134, 253–272.
- Hayward, S.A. and Salje, E.K.H. (1998) Low-temperature phase diagrams: nonlinearities due to quantum mechanical saturation of order parameters. *Journal of Physics: Condensed Matter*, 10, 1421–1430.
- (1999) Cubic-tetragonal phase transition in $SrTiO_3$ revisited: Landau theory and transition mechanism. *Phase Transitions*, 68, 501–522.
- Howard, C.J., Withers, R.L., and Kennedy, B.J. (2001) Space group and structure for the perovskite $Ca_{0.5}Sr_{0.5}TiO_3$. *Journal of Solid State Chemistry*, 160, 8–12.
- Jackson, I. (2000) Laboratory measurement of seismic wave dispersion and attenuation: Recent Progress. In S. Karato, A.M. Forte, R.C. Liebermann, G. Masters, and L. Stixrude, Eds., *Earth's Deep Interior – Mineral Physics and Tomography from the Atomic to the Global Scale*. American Geophysical Union, Washington, D.C.
- Jackson, I., Fitz Gerald, J.D., Faul, U.H., and Tan, B.H. (2003) Grain-size sensitive seismic-wave attenuation in polycrystalline olivine. *Journal of Geophysical Research*, in press.
- Karato, S. and Spetzler, H.A. (1990) Defect microdynamics in minerals and solid state mechanisms of seismic wave attenuation and velocity dispersion in the mantle. *Reviews in Geophysics*, 28, 399–421.
- Kennedy, B.J., Howard, C.J., and Chakoumakos, B.C. (1999) Phase transitions in perovskite at elevated temperatures - a powder neutron diffraction study. *Journal of Physics: Condensed Matter*, 11, 1479–1488.
- Kityk, A.V., Schranz, W., Sondergeld, P., Havlik, D., Salje, E.K.H., and Scott, J.F. (2000) Low-frequency superelasticity and nonlinear elastic behaviour of $SrTiO_3$ crystals. *Physical Review B*, 61, 946–956.
- Menard, K.P. (1999) *Dynamical mechanical analysis - A practical introduction*. CRC Press, Boca Raton, 208 pp.
- Meyer, B. and Vanderbilt, D. (2002) Ab initio study of ferroelectric domain walls in $PbTiO_3$. *Physical Review B*, 65, 104111.
- Nowick, A.S. and Berry, B.S. (1972) *Anelastic relaxation in crystalline solids*. Academic Press, New York, 677pp.
- Qin, S., Becerro, A.I., Seifert, F., Gottsmann, J., and Jiang, J. (2000) Phase transitions in $Ca_{1-x}Sr_xTiO_3$ perovskites: effects of composition and temperature. *Journal of Materials Chemistry*, 10, 1609–1615.
- Ranjan, R. and Pandey, D. (1999) Novel structural features and phase transition behaviour of $(Sr_{1-x}Ca_x)TiO_3$: II. X-ray diffraction studies. *Journal of Physics: Condensed Matter*, 11, 2247–2258.
- (2001a) Antiferroelectric phase transition in $(Sr_{1-x}Ca_x)TiO_3$ ($0.12 < x < 0.40$): I. Dielectric studies. *Journal of Physics: Condensed Matter*, 13, 4239–4249.
- (2001b) Antiferroelectric phase transition in $(Sr_{1-x}Ca_x)TiO_3$ ($0.12 < x < 0.40$): II. X-ray diffraction studies. *Journal of Physics: Condensed Matter*, 13, 4251–4266.
- Ranjan, R., Pandey, D., Siruguri, V., Krishna, P.R.S., and Paranjpe, S.K. (1999) Novel structural features and phase transition behaviour of $(Sr_{1-x}Ca_x)TiO_3$: I. Neutron diffraction study. *Journal of Physics: Condensed Matter*, 11, 2233–2246.
- Redfern, S.A.T. (1996) High-temperature structural phase transitions in perovskite ($CaTiO_3$). *Journal of Physics: Condensed Matter*, 8, 8267–8275.
- Salje, E.K.H., Gallardo, M.C., Jiménez, J., Romero, F.J., and del Cerro, J. (1998) The cubic-tetragonal phase transition in strontium titanate: excess specific heat measurements and evidence for a near-tricritical, mean field type transition mechanism. *Journal of Physics: Condensed Matter*, 10, 1161–1176.
- Schranz, W. (1997) Dynamical mechanical analysis - a powerful tool for the study of phase transitions. *Phase Transitions*, 64, 103–114.
- Wang, C., Fang, Q.F., Shi, Y., and Zhu, Z.G. (2001) Internal friction study on oxygen vacancies and domain walls in $Pb(Zr,Ti)O_3$ ceramics. *Materials Research Bulletin*, 36, 2657–2665.
- Wang, X.P. and Fang, Q.F. (2002) Mechanical and dielectric relaxation studies on the mechanism of oxygen ion diffusion in $La_2Mo_2O_9$. *Physical Review B*, 65, 064304.
- Wang, Y.N., Huang, Y.N., Shen, H.M., and Zhang, Z.F. (1996) Mechanical and dielectric energy loss related to the viscous motion and freezing of domain walls. *Journal de Physique IV, Colloque C8, supplement to Journal de Physique III*, 6, 505–514.
- Warren, W.L., Vanheusden, K., Dimos, D., Pike, G.E., and Tuttle, B.A. (1996) Oxygen vacancy motion in perovskite oxides. *Journal of the American Ceramic Society*, 79, 536–538.
- Yamanaka, T., Hirai, N., and Komatsu, Y. (2002) Structure change of $Ca_{1-x}Sr_xTiO_3$ perovskite with composition and pressure. *American Mineralogist*, 87, 1183–1189.
- Yan, F., Wang, Y., Liu, J., Zhang, Z., and Chen, X. (1999) Mechanical relaxation in $SrBi_2Ta_2O_9$ ceramics. *Journal of Applied Physics*, 74, 2794–2796.

MANUSCRIPT RECEIVED SEPTEMBER 16, 2002

MANUSCRIPT ACCEPTED NOVEMBER 1, 2002

MANUSCRIPT HANDLED BY ALISON PAWLEY